DOI: 10.1002/asia.201000111

Use of Side-Chain Incompatibility for Tailoring Long-Range p/n Heterojunctions: Photoconductive Nanofibers Formed by Self-Assembly of an Amphiphilic Donor–Acceptor Dyad Consisting of Oligothiophene and Perylenediimide

Wei-Shi Li,*[a] Akinori Saeki,[b] Yohei Yamamoto,[c] Takanori Fukushima,*[d] Shu Seki,[b] Noriyuki Ishii,[e] Kenichi Kato,[f] Masaki Takata,[f] and Takuzo Aida*[c]

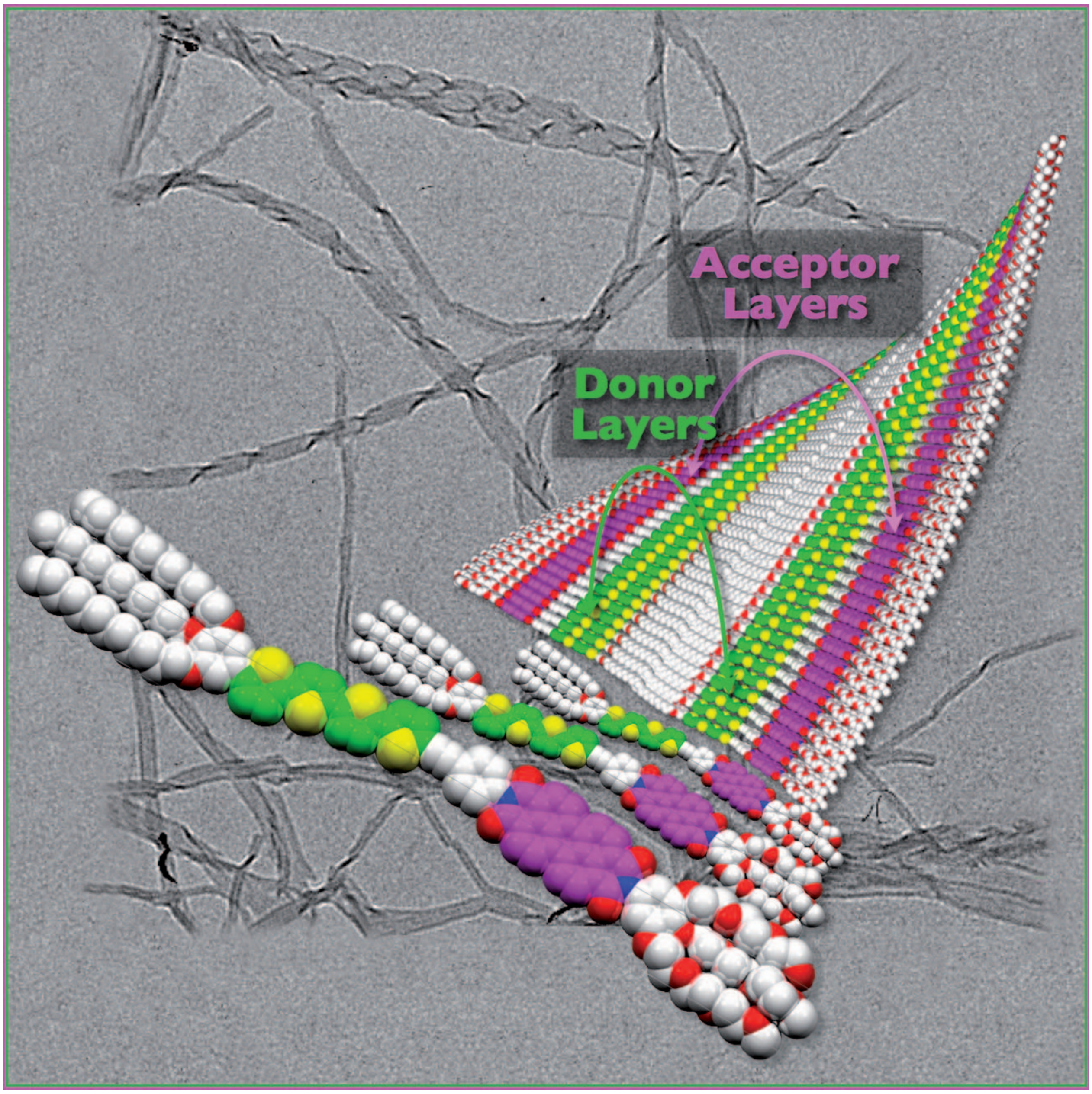

Abstract: To tailor organic p/n heterojunctions with molecular-level precision, a rational design strategy using side-chain incompatibility of a covalently connected donor–acceptor (D–A) dyad has been successfully carried out. An oligothiophene–perylenediimide dyad, when modified with triethylene glycol side chains at one terminus and dodecyl side chains at the other ($\mathbf{2}_{\mathbf{Amphi}}$), self-assembles into nanofibers with a long-range D/A heterojunction. In contrast, when the dyad is modified with dodecyl side chains at both termini ($\mathbf{2}_{\mathbf{Lipo}}$), ill-defined microfibers result. In steady-state measurements using microgap electrodes, a cast film of the nanofiber of $\mathbf{2}_{\mathbf{Amphi}}$ displays far better photoconducting properties than that of the microfiber of $\mathbf{2}_{\mathbf{Lipo}}$. Flash-photolysis time-resolved microwave conductivity measurements, in conjunction with transient absorption spectroscopy, clearly indicate that the nanofiber of $\mathbf{2}_{\mathbf{Amphi}}$ intrinsically allows for better carrier generation and transport properties than the microfibrous assembly of $\mathbf{2}_{\mathbf{Lipo}}$.

Keywords: amphiphiles · heterojunctions · nanostructures · photoconduction · self-assembly

Introduction

Remarkable advances in synthetic organic chemistry have made it possible to design a wide variety of π-conjugated molecules with attractive electronic functions for organic devices.[1–4] However, without proper molecular design that allows for long-range ordering of π-conjugated molecules, the resulting devices rarely show expected performances. This issue is particularly important for the development of thin-film organic photovoltaic devices, since they require electron-donor (D) and -acceptor (A) molecules to assemble homotropically to form a heterojunction.[1,5–7] Furthermore, for achieving a highly efficient photoinduced charge separation, the resultant p- and n-type semiconducting domains must be connected at a wide interface. However, in general, D and A components tend to assemble together by means of a charge-transfer (CT) interaction,[8] unfavorable for photoelectric conversion. To overcome this essential problem, we proposed a molecular design strategy using 'side-chain incompatibility' (Figure 1).[9] The basic motif of this strategy is a covalently connected D–A dyad ($\mathbf{1}_{\mathbf{D\text{–}A}}$), site-specifically functionalized with two incompatible side chains. Dyad $\mathbf{1}_{\mathbf{D\text{–}A}}$ likely forms a π-stack architecture with molecules on top of each other with an alternating geometry due to an intermolecular CT interaction. However, this geometry requires two incompatible side chains to mix, thereby causing a thermodynamic instability in the assembly. Consequently, $\mathbf{1}_{\mathbf{D\text{–}A}}$ prefers to stack homotropically in terms of its D and A units. Overall, the p- and n-type semiconducting molecular layers could form and be conjugated together at a very wide interface. This strategy seems to work for the formation of a D/A heterojunction in bulk materials. In fact, we demonstrated that a covalent D–A dyad consisting of oligothiophene and C_{60} units, when properly functionalized at its termini with long alkyl and oxyethylene side chains, self-assembles into a photoconductive smectic liquid crystal (LC) with a layered p/n heterojunction.[9]

In the present study, we synthesized, from oligothiophene (OT) and perylenediimide (PDI), covalently linked D–A dyads $\mathbf{2}_{\mathbf{Amphi}}$ and $\mathbf{2}_{\mathbf{Lipo}}$ (Figure 2),[10] which bear at their termini incompatible and compatible side chains, respectively. Whereas C_{60} is spherical and tends to aggregate homotropically, PDI is planar and known to form CT complexes with various electron donors.[8c,11] Hence, we thought that dyads **2** could be more appropriate than those with C_{60}[9] for discussing the general versatility of our design strategy for making a heterojunction. We found that both dyads **2** self-assemble into fibrous structures rather than LC, in which the assembly of $\mathbf{2}_{\mathbf{Amphi}}$ that has two incompatible side chains exhibits a much greater photoconducting output than that of $\mathbf{2}_{\mathbf{Lipo}}$ with the compatible side chains.

Results and Discussion

Compounds $\mathbf{2}_{\mathbf{Amphi}}$ and $\mathbf{2}_{\mathbf{Lipo}}$ were synthesized by Sonogashira coupling of an ethynyl-group-terminated OT derivative with the corresponding iodophenyl-group-appended PDI derivatives, respectively (see the Supporting Information). These

---

[a] Prof. Dr. W.-S. Li
Shanghai Institute of Organic Chemistry, Chinese Academy of Sciences
345 Ling-Ling Road, Shanghai 200032 (China)
Fax: (+86) 21-5492-5381
E-mail: liws@mail.sioc.ac.cn

[b] Dr. A. Saeki, Prof. Dr. S. Seki
Graduate School of Engineering, Osaka University
and PRESTO, Japan Science and Technology Agency (JST)
2-1 Yamadaoka, Suita, Osaka 565-0871(Japan)

[c] Dr. Y. Yamamoto, Prof. Dr. T. Aida
ERATO-SORST Nanospace Project, Japan Science and Technology Agency (JST)
National Museum of Emerging Science and Innovation
2-3-6 Aomi, Koto-ku, Tokyo 135-0064 (Japan)
Fax: (+81) 3-5841-7310
E-mail: aida@macro.t.u-tokyo.ac.jp

[d] Dr. T. Fukushima
Advanced Science Institute, RIKEN
2-1 Hirosawa, Wako, Saitama 351-0198 (Japan)
Fax: (+81) 48-467-8214
E-mail: fukushima@riken.jp

[e] Dr. N. Ishii
National Institute of Advanced Industrial Science and Technology (AIST)
Tsukuba Central-6, 1-1-1 Higashi, Tsukuba, Ibaraki 305-8566 (Japan)

[f] Dr. K. Kato, Prof. Dr. M. Takata
RIKEN SPring-8 Center
1-1-1 Kouto, Sayo-cho, Sayo-gun, Hyogo 679-5148 (Japan)

Supporting information for this article is available on the WWW under http://dx.doi.org/10.1002/asia.201000111.

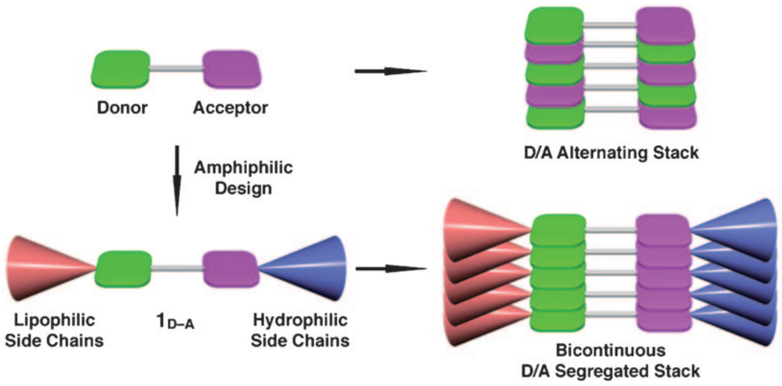

Figure 1. Schematic illustration of the design strategy using side-chain incompatibility to generate D/A heterojunctions.

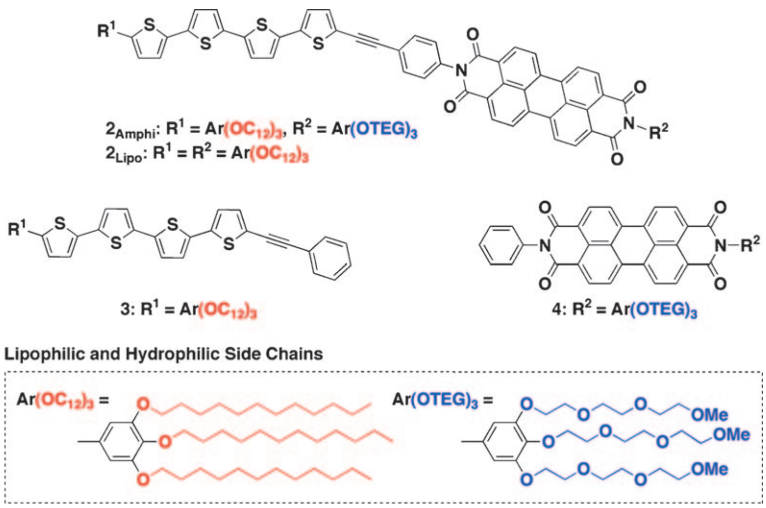

Figure 2. Molecular structures of $\mathbf{2}_{\mathrm{Amphi}}$ and $\mathbf{2}_{\mathrm{Lipo}}$, and reference compounds **3** and **4**.

dyad molecules are structurally different from one another only in their terminal side chains (Figure 2). As shown in Figure 3a, a solution of $\mathbf{2}_{\mathrm{Amphi}}$ in CH_2Cl_2 displayed absorption bands due to the PDI unit at 458, 490, and 526 nm, and that due to the OT unit at 434 nm. As expected, this absorption spectrum is essentially the same as that of $\mathbf{2}_{\mathrm{Lipo}}$. Furthermore, they are identical to the superposition of the absorption spectra of reference compounds **3** and **4** (Figures 2 and 3a). Therefore, in CH_2Cl_2, neither an intramolecular nor an intermolecular electronic interaction operates between the OT and PDI units in **2**. When excited at 430 nm, OT **3** showed an intense fluorescence (see the Supporting Information). However, when $\mathbf{2}_{\mathrm{Amphi}}$ or $\mathbf{2}_{\mathrm{Lipo}}$ was excited at 430 nm, the fluorescence of the OT unit was quenched almost completely (98 %; see the Supporting Information). Likewise, by reference to the fluorescence intensity of PDI **4**, nearly complete quenching was observed for the PDI fluorescence upon excitation of $\mathbf{2}_{\mathrm{Amphi}}$ or $\mathbf{2}_{\mathrm{Lipo}}$ at 490 nm (see the Supporting Information). These results indicate the occurrence of an efficient photoinduced electron transfer between the OT and PDI units.

Unlike previously reported OT–C_{60} dyads,[9] newly designed dyads **2** did not show a LC mesophase when analyzed using differential scanning calorimetry (DSC; see the Supporting Information). However, $\mathbf{2}_{\mathrm{Amphi}}$ in appropriate solutions self-assembled into well-defined nanofibers. Typically, a suspension of $\mathbf{2}_{\mathrm{Amphi}}$ (0.5 mg) in THF/MeOH (9:1 v/v, 1 mL) was heated at 60 °C until it turned clear. Then, the resulting solution was allowed to cool to 25 °C, whereupon a suspension again resulted. Scanning electron microscopy (SEM) of the suspension, after being air-dried, showed the presence of nanofibers with a high aspect ratio (Figure 4a). Transmission electron microscopy (TEM) allowed us to confirm that the nanofibers adopt a tapelike morphology with a width of 13–15 nm (Figure 4a, inset). It is noteworthy that a cast film of the suspension showed redshifted absorption bands due to the PDI unit [e.g., in CH_2Cl_2: 526 nm (first vibronic band)→536 nm; $\Delta\lambda = +10$ nm], whereas the absorption due to the OT unit was blueshifted (in CH_2Cl_2: 434 nm→406 nm; $\Delta\lambda = -28$ nm) (Figure 3a and b). These observations suggest that $\mathbf{2}_{\mathrm{Amphi}}$ forms a π-stack architecture in such a way that the PDI and OT units form *J*- and *H*-type aggregates, respectively.

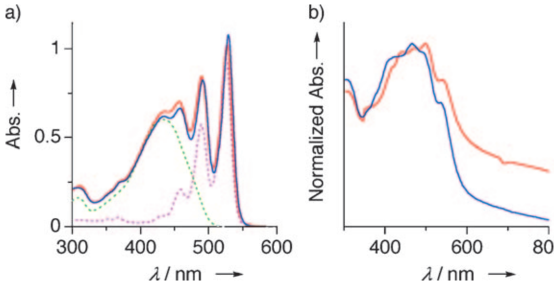

Figure 3. a) Electronic absorption spectra of $\mathbf{2}_{\mathrm{Amphi}}$ (blue), $\mathbf{2}_{\mathrm{Lipo}}$ (red), **3** (green), and **4** (purple) in CH_2Cl_2 (10 μM) at 25 °C. b) Electronic absorption spectra of cast films of self-assembled $\mathbf{2}_{\mathrm{Amphi}}$ (blue) and $\mathbf{2}_{\mathrm{Lipo}}$ (red).

X-ray diffraction (XRD) analysis of a nanofiber sample of $\mathbf{2}_{\mathrm{Amphi}}$ showed diffraction peaks in a small-angle region

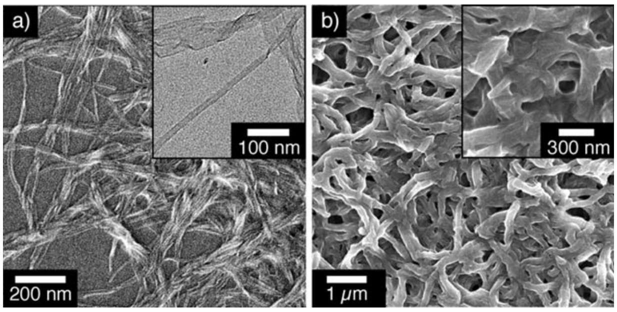

Figure 4. a) SEM and TEM (inset) micrographs of an air-dried suspension of self-assembled **2**$_{\mathbf{Amphi}}$. b) SEM micrographs of an air-dried suspension of self-assembled **2**$_{\mathbf{Lipo}}$.

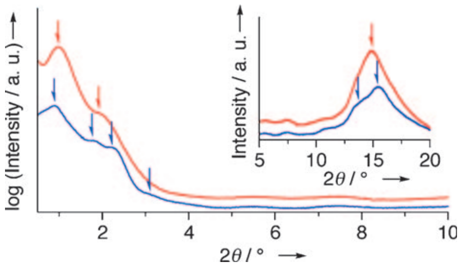

Figure 5. XRD patterns of self-assembled **2**$_{\mathbf{Amphi}}$ (blue) and **2**$_{\mathbf{Lipo}}$ (red). The inset shows XRD patterns for a wide-angle region.

(Figure 5) with *d* spacings of 6.80, 3.31, 2.67, and 1.89 nm, which can be assigned to the second-, fourth-, fifth-, and seventh-order diffractions, respectively, provided that the first-order diffraction appears with a *d* spacing of 13.6 nm. In addition to these characteristic peaks, broad peaks around 13.5 and 15.6° (Figure 5, inset) were observed, which are considered to be the TEG and alkyl halo diffractions. Thus, it is most likely that these side chains are segregated in the nanofiber to form individual layers. Note that the molecular length of **2**$_{\mathbf{Amphi}}$, as estimated by a CPK space-filling model, is approximately 8 nm. Together with the fact that the nanofiber adopts a tapelike morphology with a width of 13–15 nm (Figure 4a, inset), the XRD profile thus observed can be explained by assuming that **2**$_{\mathbf{Amphi}}$ in the nanofiber self-assembles into a bilayer configuration consisting of laterally connected tail-to-tail pairs (Figure 6a). Infrared spectroscopy of the nanofiber sample of **2**$_{\mathbf{Amphi}}$ on a KBr plate displayed CH_2 stretching vibrations at 2919 (ν_{anti}) and 2851 cm^{-1} (ν_{sym}), which indicate that the lipophilic side chains in the nanofiber adopt an extended conformation.[12] All the spectral and structural features described above allow us to conclude that the strategy of side-chain incompatibility that we employed for the controlled assembly of the OT–C_{60} dyad[9] also operates successfully in the self-assembly of **2**$_{\mathbf{Amphi}}$, thus giving rise to a D/A heterojunction.

In sharp contrast to **2**$_{\mathbf{Amphi}}$, dyad **2**$_{\mathbf{Lipo}}$, upon heating followed by cooling in THF/MeOH (e.g., 2:1 v/v), assembles into ill-defined microscopic fibers (Figure 4b) that exhibit absorption bands due to the PDI and OT units (Figure 3b) that are redshifted to 540 nm ($\Delta\lambda = +14$ nm) and blueshifted to 418 nm ($\Delta\lambda = -16$ nm), respectively, from those of **2**$_{\mathbf{Lipo}}$ in CH_2Cl_2 (Figure 3a). Hence, analogous to the nanofiber of **2**$_{\mathbf{Amphi}}$, the microfiber of **2**$_{\mathbf{Lipo}}$ likely contains *J*-aggregated PDI and *H*-aggregated OT units. However, when compared with the case of the nanofiber of **2**$_{\mathbf{Amphi}}$, the observed blueshift for OT is much less, while the redshifts for PDI are just a little larger. These observations suggest that the offset geometry of the core part of **2**$_{\mathbf{Lipo}}$ is more pronounced than that of **2**$_{\mathbf{Amphi}}$ in the nanofiber. Furthermore, a very broad absorption band around 700 nm, observed for the microfiber of **2**$_{\mathbf{Lipo}}$ (Figure 3b), is suggestive of the occurrence of a CT interaction, that is, formation of alternating D/A stacking. Consistently, XRD of self-assembled **2**$_{\mathbf{Lipo}}$ displayed only two diffraction peaks in a small-angle region with *d* spacings of 6.25 and 3.09 nm (Figure 5), which are assignable to the first- and second-order diffractions of a lamellar structure with a periodicity corresponding to the molecular length of **2**$_{\mathbf{Lipo}}$ (Figure 6b).[9]

We found that the photoconducting properties of the nanofibrous assembly of **2**$_{\mathbf{amphi}}$ are much better than those of the microfibrous assembly of **2**$_{\mathbf{Lipo}}$ (Figure 7a). For example, upon exposure to xenon light under an applied voltage of +2 V, a cast film of the nanofiber of **2**$_{\mathbf{Amphi}}$ showed a photocurrent of 4.3 nA. Under identical conditions to the above, a photocurrent, generated in a cast film of self-assembled **2**$_{\mathbf{Lipo}}$, was only 1.9×10^{-3} nA. Considering that the fluorescence quenching efficiencies of **2**$_{\mathbf{Amphi}}$ and **2**$_{\mathbf{Lipo}}$ are equally high in CH_2Cl_2 (see the Supporting Information), the con-

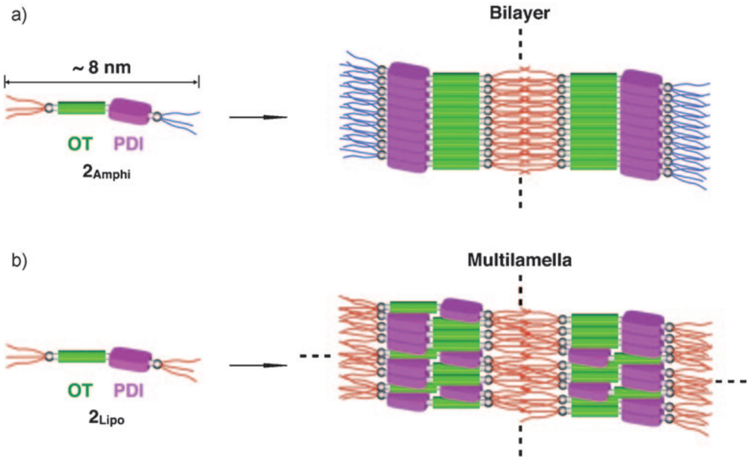

Figure 6. Schematic representations of plausible molecular packing geometries of a) the nanofiber of **2**$_{\mathbf{Amphi}}$ and b) the microfiber of **2**$_{\mathbf{Lipo}}$.

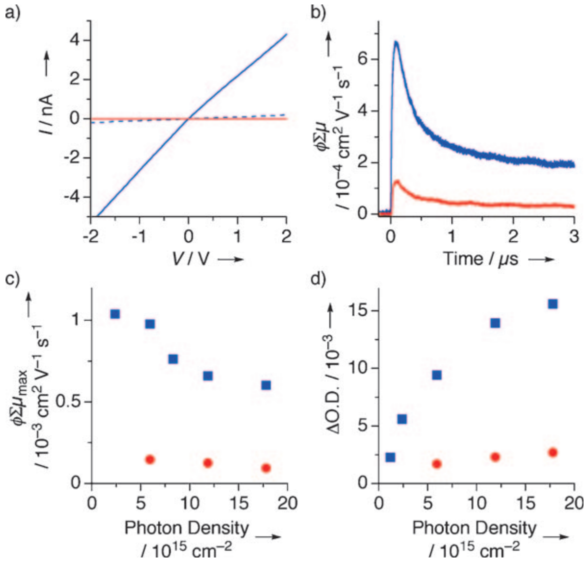

Figure 7. Photoconducting properties of cast films of self-assembled $\mathbf{2}_{\mathbf{Amphi}}$ (blue) and $\mathbf{2}_{\mathbf{Lipo}}$ (red). a) *I*/*V* profiles without (broken curves) and with photoirradiation (solid curves). b) FP-TRMC profiles ($\lambda_{ex} = 355$ nm, laser density $= 1.19 \times 10^{16}$ photons cm^{-2}). c) Plots of $\phi\Sigma\mu_{max}$ versus photon density. d) Plots of changes in transient absorption intensity (ΔO.D.) at 720 nm versus photon density.

trasting electrical properties should arise from the difference in their packing behavior (see above). We conducted flash-photolysis time-resolved microwave conductivity (FP-TRMC) measurements, which allow the motion of photocarriers under a rapidly oscillating electric field to be probed (ca. 100 ps).[13] Because of this probing function, the FP-TRMC technique does not require electrodes for charge injection, so one can evaluate the intrinsic dynamics of mobile carriers. Upon exposure at 25 °C to a 355 nm laser pulse with an intensity of 1.19×10^{16} photons cm^{-2}, a cast film of the nanofiber of $\mathbf{2}_{\mathbf{Amphi}}$ exhibited a maximum transient conductivity ($\phi\Sigma\mu_{max}$) of 6.6×10^{-4} cm^2 V^{-1} s^{-1} (Figure 7b). This value was fivefold greater than that observed for a cast film of the assembly of $\mathbf{2}_{\mathbf{Lipo}}$ (1.3×10^{-4} cm^2 V^{-1} s^{-1}). Even when the laser intensity was varied over a wide range, the nanofiber of $\mathbf{2}_{\mathbf{Amphi}}$ always showed a higher transient conductivity than the microfiber of $\mathbf{2}_{\mathbf{Lipo}}$ (Figure 7c). To further investigate the carrier generation process, we performed transient absorption spectroscopy (TAS) of the cast films of **2**. PDI anion radical species have been reported to give a transient absorption band at 720 nm.[14] Upon laser excitation at 355 nm (photon density $= 1.19 \times 10^{16}$ photons cm^{-2}), a cast film of the nanofiber of $\mathbf{2}_{\mathbf{Amphi}}$ showed a transient absorption band around 720 nm (see the Supporting Information),[15] which, however, is much broader than that observed for the reported examples.[14] The significant broadening is possibly caused by π-stacking of the PDI units.[14b] Note that such a transient absorption was less pronounced for the cast film of the microfiber of $\mathbf{2}_{\mathbf{Lipo}}$ (see the Supporting Information). Furthermore, its intensity was obviously lower than that observed for the nanofiber of $\mathbf{2}_{\mathbf{Amphi}}$ (see the Supporting Information). Even when the photon density was changed from 5.93×10^{15} to 1.78×10^{16} photons cm^{-2}, the nanofiber of $\mathbf{2}_{\mathbf{Amphi}}$ always showed a much larger transient absorption intensity at 720 nm than the microfiber of $\mathbf{2}_{\mathbf{Lipo}}$ (Figure 7d). All the transient profiles described above indicate that the nanofibrous assembly of $\mathbf{2}_{\mathbf{Amphi}}$ with a high geometrical integrity at the molecular level intrinsically provides better carrier generation and transport properties than the microfibrous assembly of $\mathbf{2}_{\mathbf{Lipo}}$ (Figure 7b–d). However, such differences cannot fully account for the far better device performance achieved with the nanofiber of $\mathbf{2}_{\mathbf{Amphi}}$ (Figure 7a). We consider that the nanofiber of $\mathbf{2}_{\mathbf{Amphi}}$ with a much better geometrical integrity for π-stacking likely gives rise to longer carrier transport pathways than the ill-defined microfibrous assembly of $\mathbf{2}_{\mathbf{Lipo}}$.

Conclusion

Through investigations of the self-assembly and photoconducting behaviors of newly designed oligothiophene–perylenediimide (OT–PDI) dyads, we confirmed that our design strategy with ‘side-chain incompatibility’ is quite promising for the realization of p/n heterojunctions from covalently connected D–A dyads. An additional bonus is that this design strategy can give rise to long-range structural integrity that is essential for excellent device performances. Elaboration of side-chain-incompatible D–A dyads in terms of absorption range and carrier transport properties is a subject worthy of further investigations for developing molecularly engineered photovoltaic devices.

Experimental Section

General

Unless otherwise noted, all commercial reagents were used as received. Tetrahydrofuran (THF) was heated at reflux with a mixture of Na and benzophenone under argon, and was freshly distilled prior to use. CH_2Cl_2 was dried with CaH_2 under argon and freshly distilled prior to use. ^{1}H and ^{13}C NMR spectra were recorded at 25 °C on a JEOL model NM-Excalibur 500 FT NMR spectrometer operating at 500 and 125 MHz, respectively; chemical shifts were determined with respect to non- or partially deuterated solvents as internal references. Matrix-assisted laser desorption ionization time-of-flight (MALDI-TOF) mass spectrometry was performed on an Applied Biosystems model Voyager-DE STR mass spectrometer using dithranol as a matrix in a reflector mode. Recycling preparative size-exclusion chromatography (SEC) was performed with $CHCl_3$ as an eluent using JAIGEL 1H (pore size: 20–30 Å), 2H (40–50 Å), and 3H (>50 Å) columns on a JAI model LC-908 recycling HPLC system equipped with a JASCO model MD-2010 variable-wavelength UV/Vis detector. Electronic absorption, fluorescence, and infrared spectra were recorded on a JASCO model V-570 UV/VIS/NIR spectrophotometer, a JASCO model FP-6500 spectrofluorometer, and a JASCO model FT/IR-610$_{plus}$ Fourier transform infrared spectrometer, respectively. Differential scanning calorimetry (DSC) was performed on a Mettler-Toledo model DSC 822^e differential scanning calorimeter. Cooling and heating profiles were recorded and analyzed using the Mettler-Toledo STAR^e software system. Scanning electron microscopy (SEM) was performed on a JEOL model JSM-6700F FE-SEM electron microscope operating at 5 kV. Transmission electron microscopy (TEM) was recorded on a Philips model Tecnai F20 electron microscope operating at 120 kV. Sample dispersions were applied onto a specimen grid covered with a thin carbon support film, which had been hydrophilized by a JEOL model HDT-400 ion bombardment device. Images were recorded on a Gatan slow scan CCD camera (Retractable Multiscan Camera) under low-dose conditions. High-resolution X-ray diffraction experiments were carried out using a synchrotron radiation X-ray beam with a wavelength of 1.08 Å on BL44B2 at the Super Photon Ring (SPring-8, Hyogo, Japan). A large Debye–Scherrer camera with the camera length of 286.48 mm was used with an imaging plate as a detector, and all diffraction patterns were obtained with a 0.01° step in 2θ. During the measurements, all samples, put into a 0.7 mm-thick glass capillary, were rotated to obtain homogeneous diffraction patterns.

Measurements of Photoconducting Properties

Photoconducting properties of self-assembled $\mathbf{2}_{\text{Amphi}}$ and $\mathbf{2}_{\text{Lipo}}$ were measured at 25 °C using a Keithley model 4200-SCS semiconductor parameter analyzer under reduced pressure ($<10^{-3}$ Pa) in a Nagase Electronic Equipment Service model GRAIL10-Helips-4-HT prober. Suspensions of self-assembled $\mathbf{2}_{\text{Amphi}}$ and $\mathbf{2}_{\text{Lipo}}$ in a THF/MeOH mixed solvent were cast onto a silicon substrate coated with a 200 nm-thick insulating silicon oxide layer. Then, Au was thermally deposited onto the resulting thin films, forming electrodes with a 50 μm separation. A xenon light source (Asahi Spectra model MAX-301) was used for photoirradiation with a light power density of 0.91 mW mm^{-2}.

FP-TRMC and TAS Measurements

FP-TRMC and TAS were measured with an identical geometry using an in situ TRMC-TAS system.[13b] In the conductivity measurements, a resonant cavity was used to obtain a high degree of sensitivity. The resonant frequency and microwave power were set at approximately 9.1 GHz and 3 mW, respectively, so that the electric field of the microwave was small enough not to disturb the thermal motion of charge carriers. Charge carriers were photochemically generated using the third-harmonic generation (THG, $\lambda = 355$ nm) light pulses from a Spectra Physics model INDY-HG Nd:YAG laser (5–8 ns pulse duration). The TRMC signal, picked up by a diode (rise time <1 ns), was monitored by a Tektronics model TDS3052B digital oscilloscope. The observed conductivities were normalized, given by a photocarrier generation yield (ϕ) multiplied by sum of the charge carrier mobilities ($\Sigma\mu$), according to an equation, $\phi\Sigma\mu = (1/eAI_0F_{\text{light}})(\Delta P_r/P_r)$, in which e, A, I_0, F_{light}, P_r, and ΔP_r denote unit charge of a single electron, sensitivity factor (S^{-1}cm), incident photon density of the excitation laser (photon cm^{-2}), filling factor (cm^{-1}), and reflected microwave power and its change, respectively. Likewise, TAS was measured using continuous white light from a xenon lamp as a probe. All the experiments were performed at 25 °C in air.

Acknowledgements

W.-S.L. thanks the financial support from Chinese Academy of Sciences, National Natural Science Foundation of China (90922019), and the Science and Technology Commission of the Shanghai Municipality (09PJ1411700). T.F. thanks MEXT, Japan, for financial support (21350108). The synchrotron radiation experiments were performed at BL44B2 in SPring-8 with the approval of RIKEN (proposal no. 20090021).

---

[1] For selected reviews on organic photovoltaics, see: a) S. Günes, H. Neugebauer, N. S. Sariciftci, *Chem. Rev.* **2007**, *107*, 1324–1338; b) B. C. Thompson, J. M. J. Fréchet, *Angew. Chem.* **2008**, *120*, 62–82; *Angew. Chem. Int. Ed.* **2008**, *47*, 58–77; c) G. Dennler, M. C. Scharber, C. J. Brabec, *Adv. Mater.* **2009**, *21*, 1323–1338; d) J. Chen, Y. Cao, *Acc. Chem. Res.* **2009**, *42*, 1709–1718; e) J. Roncali, *Acc. Chem. Res.* **2009**, *42*, 1719–1730; f) Y.-J. Cheng, S.-H. Yang, C.-S. Hsu, *Chem. Rev.* **2009**, *109*, 5868–5923.

[2] For selected reviews on organic light-emitting diodes, see: a) T. Baumgartner, R. Réau, *Chem. Rev.* **2006**, *106*, 4681–4727; b) Y. Shirota, H. Kageyama, *Chem. Rev.* **2007**, *107*, 953–1010; c) J. Roncali, P. Leriche, A. Cravino, *Adv. Mater.* **2007**, *19*, 2045–2060.

[3] For selected reviews on organic field-effect transistors, see: a) J. Zaumseil, H. Sirringhaus, *Chem. Rev.* **2007**, *107*, 1296–1323; b) S. Allard, M. Forster, B. Souharce, H. Thiem, U. Scherf, *Angew. Chem.* **2008**, *120*, 4138–4167; *Angew. Chem. Int. Ed.* **2008**, *47*, 4070–4098; c) A. L. Rogach, N. Gaponik, J. M. Lupton, C. Bertoni, D. E. Gallardo, S. Dunn, N. L. Pira, M. Paderi, P. Repetto, S. G. Romanov, C. O'Dwyer, C. M. S. Torres, A. Eychmüller, *Angew. Chem.* **2008**, *120*, 6638–6650; *Angew. Chem. Int. Ed.* **2008**, *47*, 6538–6549; d) D. Braga, G. Horowitz, *Adv. Mater.* **2009**, *21*, 1473–1486; e) S. Liu, W. M. Wang, A. L. Briseno, S. C. B. Mannsfeld, Z. Bao, *Adv. Mater.* **2009**, *21*, 1217–1232.

[4] For selected reviews on organic sensors, see: a) S. W. Thomas III, G. D. Joly, T. M. Swager, *Chem. Rev.* **2007**, *107*, 1339–1386; b) C. McDonagh, C. S. Burke, B. D. MacCraith, *Chem. Rev.* **2008**, *108*, 400–422; c) F. Feng, F. He, L. An, S. Wang, Y. Li, D. Zhu, *Adv. Mater.* **2008**, *20*, 2959–2964.

[5] a) L.-M. Chen, Z. Hong, G. Li, Y. Yang, *Adv. Mater.* **2009**, *21*, 1434–1449; b) J. Peet, M. L. Senatore, A. J. Heeger, G. C. Bazan, *Adv. Mater.* **2009**, *21*, 1521–1527; c) J.-L. Brédas, J. E. Norton, J. Cornil, V. Coropceanu, *Acc. Chem. Res.* **2009**, *42*, 1691–1699; d) J. Peet, A. J. Heeger, G. C. Bazan, *Acc. Chem. Res.* **2009**, *42*, 1700–1708; e) P. Heremans, D. Cheyns, B. P. Rand, *Acc. Chem. Res.* **2009**, *42*, 1740–1747; f) W. J. Potscavage, Jr., A. Sharma, B. Kippelen, *Acc. Chem. Res.* **2009**, *42*, 1758–1767; g) X.-Y. Zhu, Q. Yang, M. Muntwiler, *Acc. Chem. Res.* **2009**, *42*, 1779–1787.

[6] a) E. Peeters, P. A. van Hal, S. C. J. Meskers, R. A. J. Janssen, E. W. Meijer, *Chem. Eur. J.* **2002**, *8*, 4470–4474; b) F. Würthner, Z. Chen, F. J. M. Hoeben, P. Osswald, C.-C. You, P. Jonkheijm, J. v. Herrikhuyzen, A. P. H. J. Schenning, P. P. A. M. van der Schoot, E. W. Meijer, E. H. A. Beckers, S. C. J. Meskers, R. A. J. Janssen, *J. Am. Chem. Soc.* **2004**, *126*, 10611–10618; c) P. Samorì, X. Yin, N. Tchebotareva, Z. Wang, T. Pakula, F. Jäckel, M. D. Watson, A. Venturini, K. Müllen, J. P. Rabe, *J. Am. Chem. Soc.* **2004**, *126*, 3567–3575; d) A. L. Sisson, N. Sakai, N. Banerji, A. Fürstenberg, E. Vauthey, S. Matile, *Angew. Chem.* **2008**, *120*, 3787–3789; *Angew. Chem. Int. Ed.* **2008**, *47*, 3727–3729; e) A. Kira, T. Umeyama, Y. Matano, K. Yoshida, S. Isoda, J. K. Park, D. Kim, H. Imahori, *J. Am. Chem. Soc.* **2009**, *131*, 3198–3200.

[7] a) Y. Yamamoto, T. Fukushima, Y. Suna, N. Ishii, A. Saeki, S. Seki, S. Tagawa, M. Taniguchi, T. Kawai, T. Aida, *Science* **2006**, *314*, 1761–1764; b) Y. Yamamoto, T. Fukushima, A. Saeki, S. Seki, S. Tagawa, N. Ishii, T. Aida, *J. Am. Chem. Soc.* **2007**, *129*, 9276–9277; c) Y. Yamamoto, G. Zhang, W. Jin, T. Fukushima, N. Ishii, A. Saeki, S. Seki, S. Tagawa, T. Minari, K. Tsukagoshi, T. Aida, *Proc. Natl. Acad. Sci. USA* **2009**, *106*, 21051–21056.

[8] a) V. Percec, M. Glodde, T. K. Bera, Y. Miura, I. Shiyanovskaya, K. D. Singer, V. S. K. Balagurusamy, P. A. Heiney, I. Schnell, A. Rapp, H.-W. Spiess, S. D. Hudsonk, H. Duan, *Nature* **2002**, *417*, 384–387; b) W. Pisula, M. Kastler, D. Wasserfallen, J. W. F. Robertson, F. Nolde, C. Kohl, K. Müllen, *Angew. Chem.* **2006**, *118*, 834–838; *Angew. Chem. Int. Ed.* **2006**, *45*, 819–823; c) P. Jonkheijm, N. Stutzmann, Z. Chen, D. M. de Leeuw, E. W. Meijer, A. P. H. J. Schenning, F. Würthner, *J. Am. Chem. Soc.* **2006**, *128*, 9535–9540.

[9] W.-S. Li, Y. Yamamoto, T. Fukushima, A. Saeki, S. Seki, S. Tagawa, H. Masunaga, S. Sasaki, M. Takata, T. Aida, *J. Am. Chem. Soc.* **2008**, *130*, 8886–8887.

[10] Photoinduced electron-transfer properties of oligothiophene–PDI dyads and triads have been reported in the following: a) L. X. Chen, S. Xiao, L. Yu, *J. Phys. Chem. B* **2006**, *110*, 11730–11738; b) J. Guo, Y. Liang, S. Xiao, J. M. Szarko, M. Sprung, M. K. Mukhopadhyay, J. Wang, L. Yu, L. X. Chen, *New J. Chem.* **2009**, *33*, 1497–1507.

[11] a) X. Guo, D. Zhang, H. Zhang, Q. Fan, W. Xu, X. Ai, L. Fan, D. Zhu, *Tetrahedron* **2003**, *59*, 4843–4850; b) Y. Zhang, L.-Z. Cai, C.-Y. Wang, G.-Q. Lai, Y.-J. Shen, *New J. Chem.* **2008**, *32*, 1968–1973; c) G. De Luca, A. Liscio, M. Melucci, T. Schnitzler, W. Pisula, C. G. Clark, Jr., L. M. Scolaro, V. Palermo, K. Müllen, P. Samorì, *J. Mater. Chem.* **2010**, *20*, 71–82.

[12] a) R. G. Snyder, H. L. Strauss, C. A. Elliger, *J. Phys. Chem.* **1982**, *86*, 5145–5150; b) N. Reitzel, D. R. Greve, K. Kjaer, P. B. Howes, M. Jayaraman, S. Savoy, R. D. McCullough, J. T. McDevitt, T. Bjørnholm, *J. Am. Chem. Soc.* **2000**, *122*, 5788–5800; c) J. P. Hill, W. Jin, A. Kosaka, T. Fukushima, H. Ichihara, T. Shimomura, K. Ito, T. Hashizume, N. Ishii, T. Aida, *Science* **2004**, *304*, 1481–1483.

[13] a) F. C. Grozema, L. D. A. Siebbeles, J. M. Warman, S. Seki, S. Tagawa, U. Scherf, *Adv. Mater.* **2002**, *14*, 228–231; b) A. Saeki, S. Seki, T. Takenobu, Y. Iwasa, S. Tagawa, *Adv. Mater.* **2008**, *20*, 920–923.

[14] a) D. Gosztola, M. P. Niemczyk, W. Svec, A. S. Lukas, M. R. Wasielewski, *J. Phys. Chem. A* **2000**, *104*, 6545–6551; b) T. van der Boom, R. T. Hayes, Y. Zhao, P. J. Bushard, E. A. Weiss, M. R. Wasielewski, *J. Am. Chem. Soc.* **2002**, *124*, 9582–9590.

[15] A OT cation radical species was barely detected in the transient absorption spectroscopy, probably due to its inherently small absorption coefficient: V. Wintgens, P. Valat, F. Garnier, *J. Phys. Chem.* **1994**, *98*, 228–232.

Received: February 8, 2010
Revised: March 13, 2010